AFCRL-70-0007
JANUARY 1970
AIR FORCE SURVEYS IN GEOPHYSICS, NO. 214

AIR FORCE CAMBRIDGE RESEARCH LABORATORIES
L. G. HANSCOM FIELD, BEDFORD, MASSACHUSETTS

REFRACTION, ATTENUATION, AND BACKSCATTERING OF ELECTROMAGNETIC WAVES IN THE TROPOSPHERE: A Revision of Chapter 9, Handbook of Geophysics and Space Environments

V. J. FALCONE, JR.
R. DYER

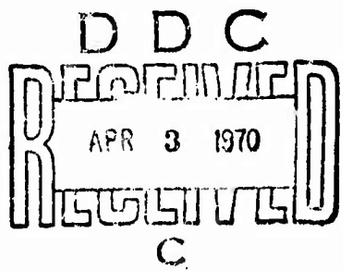

OFFICE OF AEROSPACE RESEARCH
United States Air Force

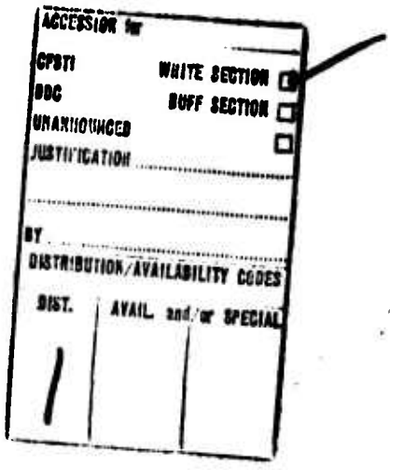

AFCRL-70-0007
JANUARY 1970
AIR FORCE SURVEYS IN GEOPHYSICS, NO. 214

ENVIRONMENTAL CONSULTATION SERVICE
AIR FORCE CAMBRIDGE RESEARCH LABORATORIES
L. G. HANSCOM FIELD, BEDFORD, MASSACHUSETTS

REFRACTION, ATTENUATION, AND BACKSCATTERING OF ELECTROMAGNETIC WAVES IN THE TROPOSPHERE: A Revision of Chapter 9, Handbook of Geophysics and Space Environments

V. J. FALCONE, JR.
R. DYER

OFFICE OF AEROSPACE RESEARCH
United States Air Force

Abstract

The need for geophysical and astrophysical information is critical for the design of aircraft, missiles, and satellites. The HANDBOOK OF GEOPHYSICS AND SPACE ENVIRONMENTS is an attempt by the U. S. Air Force to organize some of these data into compact form.

The effects of the lower atmosphere on propagation of electromagnetic waves in the optical, microwave, and radio regions are discussed in this Chapter; the emphasis is on information useful in meteorological investigations.

BLANK PAGE

Contents

Illustrations

REFRACTION, ATTENUATION, AND BACKSCATTERING OF ELECTROMAGNETIC WAVES IN THE TROPOSPHERE: A Revision of Chapter 9, Handbook of Geophysics and Space Environments

9.1 REFRACTION IN THE LOWER TROPOSPHERE by V.J. Falcone, Jr.

The speed of propagation of an electromagnetic wave in free space is a constant, c, which is equal to 3×10^8 m/sec. In a material medium, such as the atmosphere, the speed of propagation varies. Even small variations in speed produce marked changes in the direction of propagation, that is refraction.

In the atmosphere, the speed of propagation varies with changes in composition, temperature, and pressure. At radio wavelengths speed does not vary significantly with the wavelength, but in the optical region the speed depends strongly on the wavelength. In the lower 15 km of the atmosphere water vapor is the major contributor to variation in atmospheric composition, and at radio wavelengths the speed of propagation is strongly affected by water vapor. Temperature and pressure variations are principally functions of altitude, although for propagation at small elevation angles significant variations may occur along horizontal distances. From the standpoint of effect on the speed of propagation, temperature variations at any given altitude are more significant than pressure variations.

(Received for publication 14 November 1969)

In its most general form the refractive index is a complex function. The real term of the complex function is called the phase refractive index, n;

$$n = \frac{c}{v} , \tag{9-1}$$

where c is the speed of light in a vacuum and v, the phase velocity, is the speed of propagation in a particular medium. In the troposphere where n is nearly equal to one, it is convenient to define the quantity

$$N = (n - 1) \times 10^6 . \tag{9-2}$$

N is called the refractive modulus; units of $(n - 1) \times 10^6$ are called N-units.

9.1.1 Optical Wavelengths

An approximate relation between the optical refractive modulus and atmospheric pressure and temperature is

$$N_\infty = 77.6 \frac{P}{T} , \tag{9-3}$$

where N_∞ is the refractive modulus for wavelengths $>> 20\mu$, P is atmospheric pressure in millibars, and T is atmospheric temperature in degrees Kelvin.

The dispersion formula of Edlen (1953), which has been adopted by the Joint Commission for Spectroscopy, is

$$N_s = 64.328 + \frac{29498.10}{146 - 1/\lambda^2} + \frac{255.40}{41 - 1/\lambda^2} , \tag{9-4}$$

where N_s is the refractive modulus at a wavelength λ for a temperature of $288^\circ K$ and a pressure of 1013.25 mb, and λ is the wavelength in microns. A somewhat less precise but more convenient dispersion formula is

$$N = N_\infty \left[1 + \frac{7.52 \times 10^{-3}}{\lambda^2} \right] . \tag{9-5}$$

Equations 9-3 and 9-5 may be combined to give the refractive modulus as a function of pressure, temperature, and wavelength;

$$N = \frac{77.6P}{T} + \frac{0.584P}{T\lambda^2} . \tag{9-6}$$

Refractive moduli calculated by using Eq. 9-6 will be in error no more than one N-unit over the temperature range -30°C to +30°C for wavelengths from 0.2μ to 20μ. Thus Eq. 9-6 covers the spectrum from the near ultraviolet through the near infrared. Figure 9-1 is a nomograph based on Eq. 9-6 that gives values of N accurate to about 5 N-units.

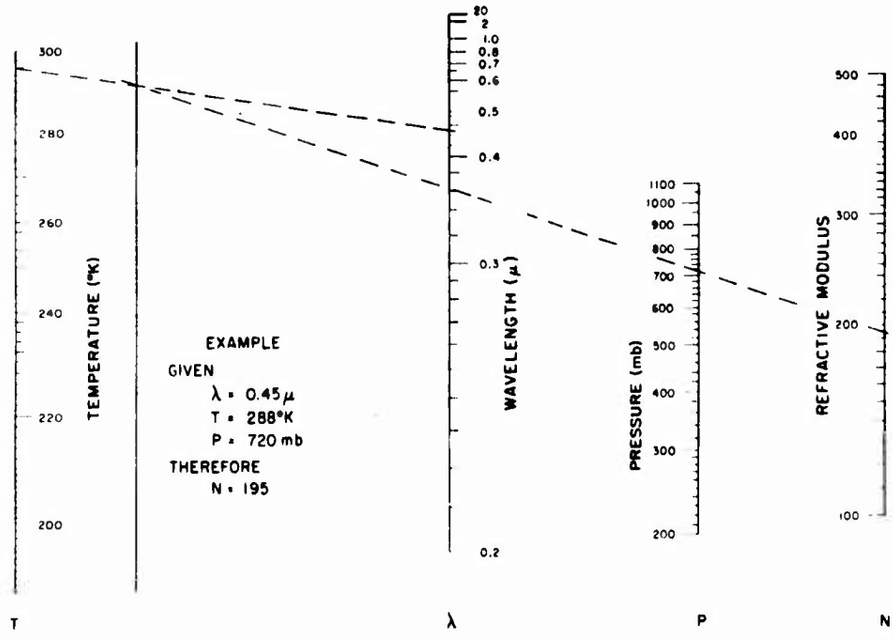

Figure 9-1. Nomograph for Computing Refractive Modulus at Optical Wavelengths

9.1.2 Radio Wavelengths

At radio wavelengths the relationship of refractive modulus to pressure, temperature, and water-vapor pressure is given by:

$$N = \frac{77.6\,P}{T} + \frac{373000\,P_{wv}}{T^2} \qquad (9\text{-}7)$$

where P_{wv} is the partial pressure of water vapor in millibars, P is pressure in millibars, and T is temperature in degrees Kelvin. Figures 9-2 and 9-3 are nomographs based on Eq. 9-7; they give values accurate to within 5 N-units.

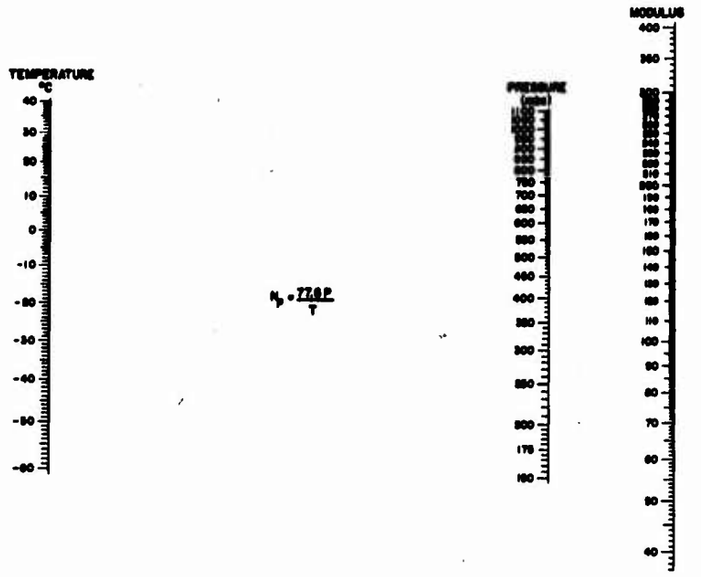

Figure 9-2. Nomograph for Computing Contribution to Microwave Refractive Modulus Due to Density of Atmospheric Gas

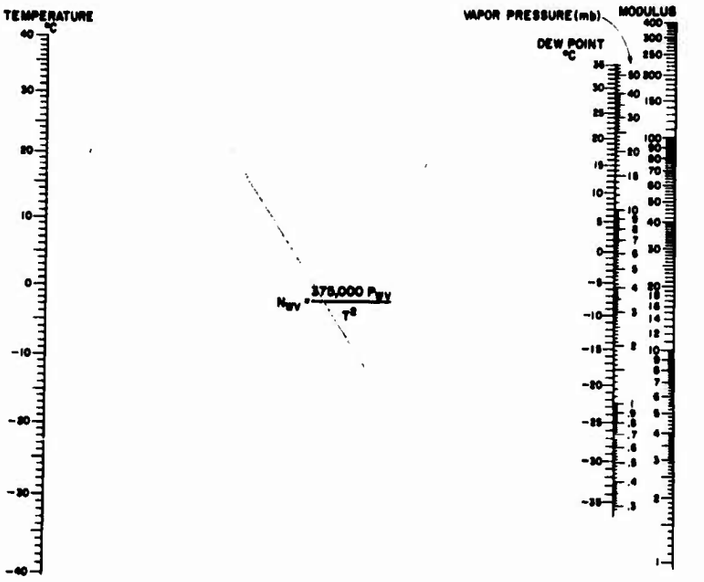

Figure 9-3. Nomograph for Computing Contribution to Microwave Refractive Modulus Due to Water Vapor

Equation 9-7 is accurate to: 0.1 N-units from the longest radio wavelengths in use down to about 6 mm (50 GHz); 5 N-units from 6 mm to 4 mm (50 to 75 GHz); and 1 N-unit from 4 mm to 2.6 mm (75 to 115 GHz).

Absorption by atmospheric constituents begins to rise to significant proportion with decreasing wavelength beyond 1.5 cm. Water vapor content is by far the leading factor in causing changes in N, followed in order of importance by temperature, and pressure. For example, for a temperature of 15°C, pressure of 1013 mb near ground level, and a relative humidity of 60 percent (P_{wv} = 10 mb), the fluctuation, ΔN, is

$$\Delta N = 4.5\Delta P_{wv} - 1.26\Delta T + 0.27\Delta P \qquad (9\text{-}8)$$

As Eq. 9-8 shows, a fluctuation in water vapor pressure has 16 times the effect on the refractive index as the same amount of fluctuation in total pressure, and 3.5 times the effect as the same fluctuation in temperature. Equation 9-7 may also be used in the windows of relative transparency for submillimeter waves ($\lambda > 100\mu$, $f < 3\times10^6$ GHz) with an error of 10 to 20 N-units.

9.1.3 Standard Profiles of Refractive Modulus

The vertical distribution of the refractive modulus can be calculated from Eq. 9-7 using vertical distributions of vapor pressure and temperature as a function of pressure.

Under normal conditions, N tends to decrease exponentially with height. An exponential decrease is usually an accurate description for heights greater than 10,000 feet (3 km); below 10,000 feet, N may depart considerably from exponential behavior. The median value for the gradient dN is typically - 0.012 N-units per foot for the first few thousand feet above ground level.

For many purposes it is desirable to have standard refractive-modulus profiles for the atmosphere. By using the equations of the model atmosphere (Chapter 2), an exact analytical expression for the standard optical refractive modulus can be derived. A simplified approximation to this is

$$N_\infty = 273 \exp(-Z/32.2), \quad (Z \leq 25); \qquad (9\text{-}9)$$

Z is the altitude in thousands of feet.

Equation 9-9 can be differentiated to obtain the standard gradient of optical refractive modulus;

$$\frac{dN_\infty}{dZ} = -8.48 \exp(-Z/32.2), \quad (Z \leq 25)\,. \qquad (9\text{-}10)$$

Equations 9-9 and 9-10 may be corrected for dispersion through use of Eq. 9-5.

For the radio wavelengths it is necessary to assume a distribution of water vapor in order to obtain an expression for the refractive modulus. Assuming $P_{wv} = 10.2\,(1 - 0.0195\,Z)^6$, for $Z \leq 25$, a simplified approximation is

$$N = 316 \exp(-Z/26.5), \quad (Z \leq 25) . \tag{9-11}$$

The standard gradient of radio-wave refractive modulus is then:

$$\frac{dN}{dZ} = -11.9 \exp(-Z/26.5), \quad (Z \leq 25) . \tag{9-12}$$

Figures 9-4 and 9-5 are graphs of standard profiles calculated from Eq. 9-10 through 9-12.

9.1.4 Variations of Refractive Moduli

Actual profiles may differ markedly from the standard profiles. Figures 9-6 through 9-9 show some profiles of refractive modulus at microwave frequencies calculated from radiosonde measurements. These are considered typical for the air masses indicated. Average deviations from a model atmosphere refractive index have been studied extensively; for example, see Bean and Dutton (1968).

Cumulus clouds are evidence of the existence of a very inhomogeneous atmosphere. Figure 9-10 shows some measurements of refractive modulus and associated parameters within a fair-weather cumulus cloud. The time response of the instruments from which refractive modulus, temperature, and water-vapor pressure were obtained was such that changes occurring in distances as small as 5 feet (1.5m) could be measured. However, the instrument for measuring liquid water content was much slower responding. Figure 9-11 shows a composite cloud which summarizes data from 30 cloud passes.

Figure 9-12 shows the average ΔN cloud to clear air to be expected in various parts of the United States at the midseason months. The chances of having cumulus clouds at 1500 h local time for these months is also shown. Additional climatological data on ΔN and cumulus clouds is given by Cunningham (1962).

The deviations in refractive modulus are principally in the vertical direction. Regions of more or less constant gradient of the refractive modulus are called stratified layers. The horizontal extent of these layers may vary from a few miles to hundreds of miles depending on the meteorological processes by which they are produced. When N decreases with height inside a specific layer much faster than it does above or below the layer, the layer is said to be super-refracting for propagation. One cause of this is temperature inversion (Section 3.1.5). Layers

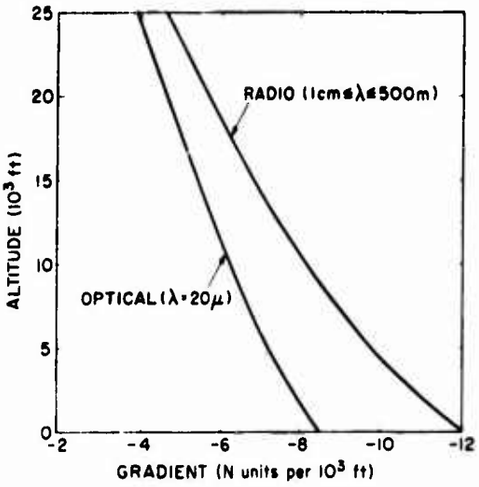

Figure 9-4. Variation of Standard Gradient of Refractive Modulus with Altitude

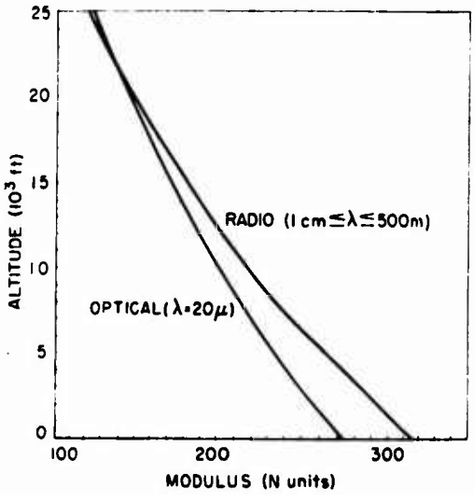

Figure 9-5. Variation of Standard Refractive Modulus with Altitude

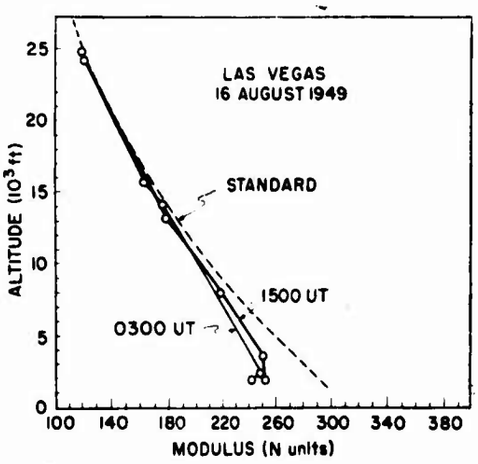

Figure 9-6. Microwave Refractive Modulus Profile in Continental Tropical Air Mass

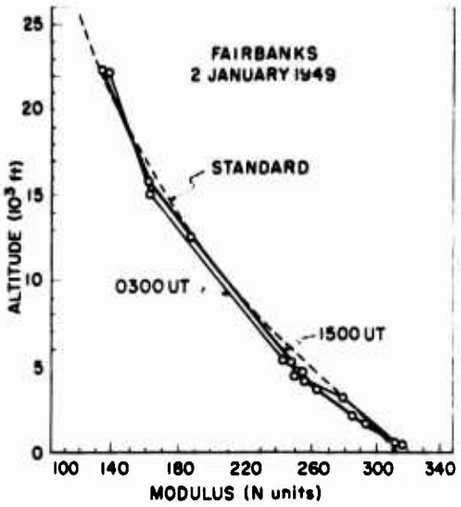

Figure 9-7. Microwave Refractive Modulus Profile in Continental Polar Air Mass

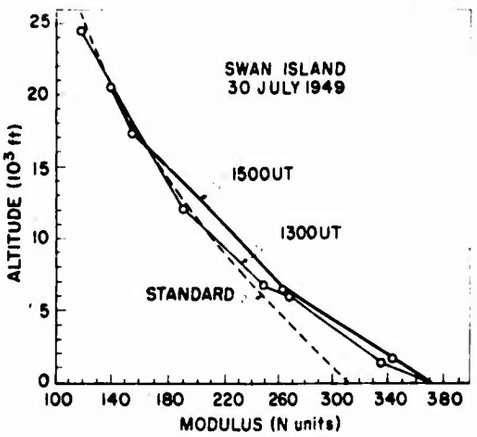

Figure 9-8. Microwave Refractive Modulus Profile in Continental Polar Air Mass

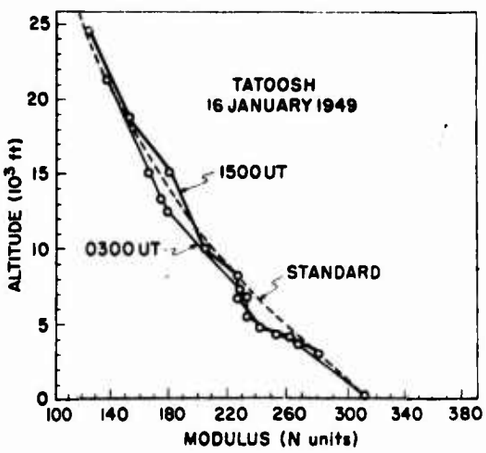

Figure 9-9. Microwave Refractive Modulus Profile in Maritime Polar Air Mass

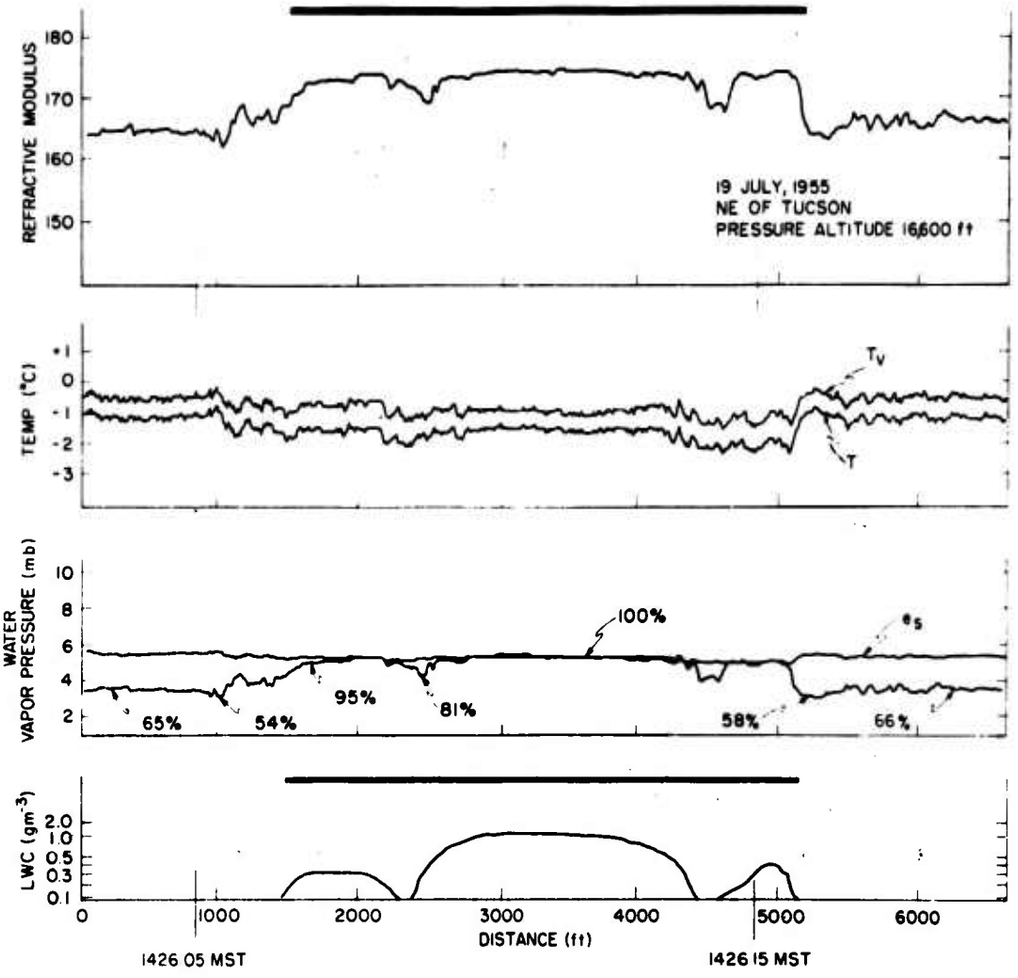

Figure 9-10. Aircraft Measurements Through a Cumulus Cloud. The heavy lines show the time during which an observer in the aircraft indicated that the plane was within the visible cloud. The calculated virtual temperature, T_V, was corrected for liquid water content; T is the measured temperature. Relative humidity in percent is shown on the ambient water-vapor pressure curve; the curve labelled e_S is the calculated saturation water-vapor pressure at the temperature encountered. The bottom curve shows the liquid water content (LWC)

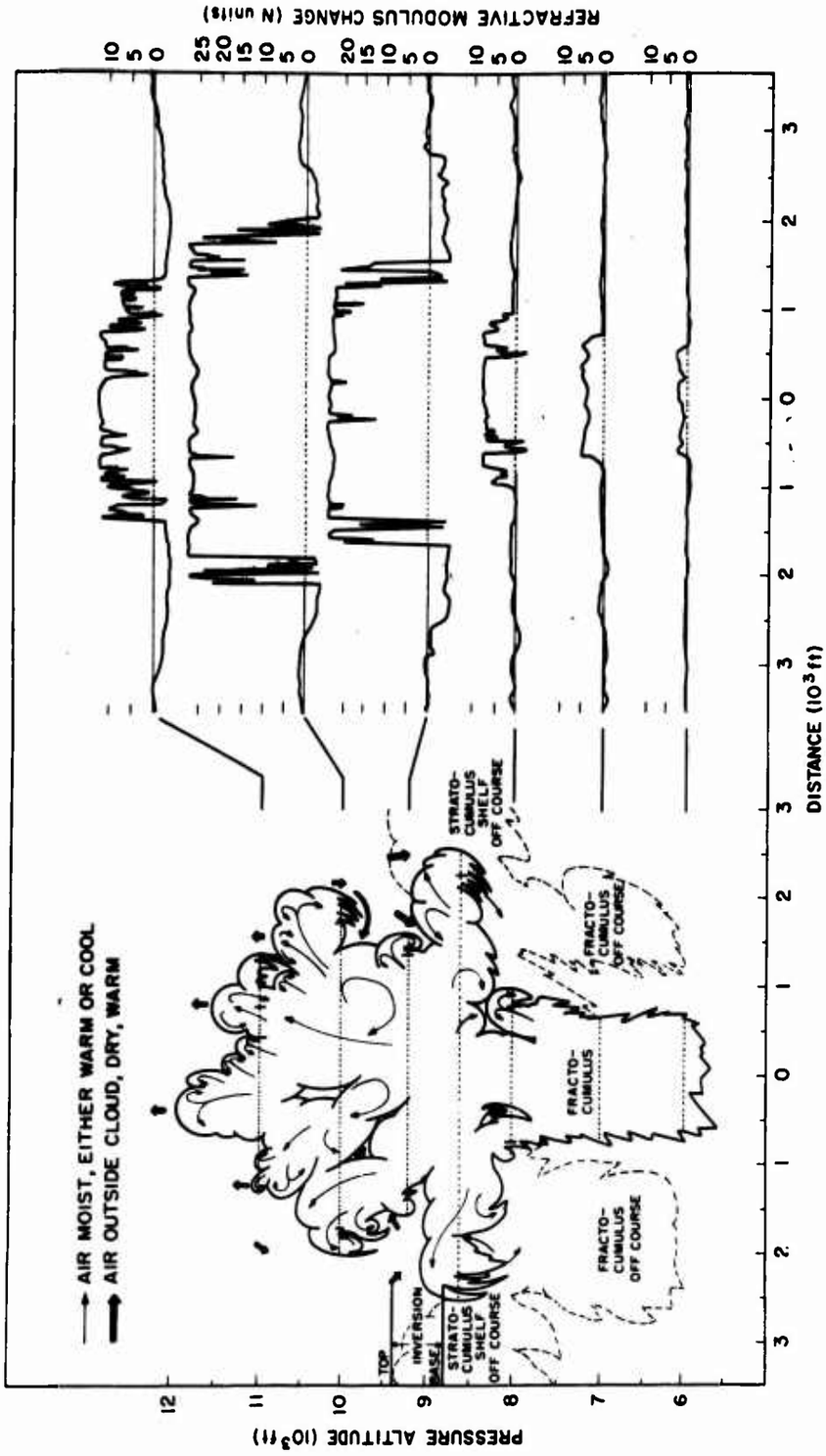

Figure 9-11. Average Cloud Shape Cross Section 90° to Wind Shear and Average Refractive Modulus Changes on June 30, 1955, NW of Boston, Mass. Composite of 30 cloud passes; air motion deduced from temperature and refractive modulus data

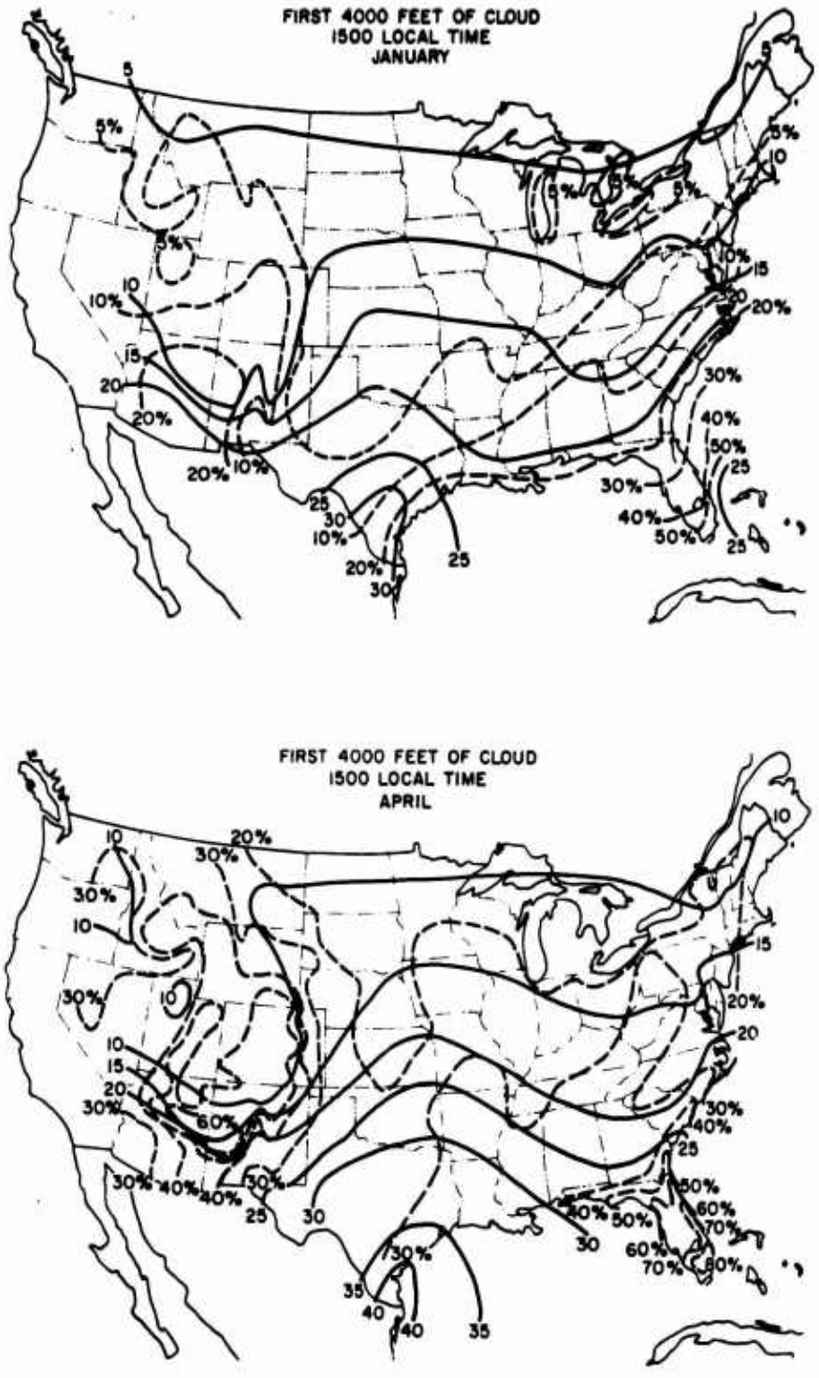

Figure 9-12. Percent Frequency of Cumulus and Cumulonibus Cloud (Dashed Contours) and Δ N, the Average Change in Refractive Modulus (Solid Contours) for January, April, July and October

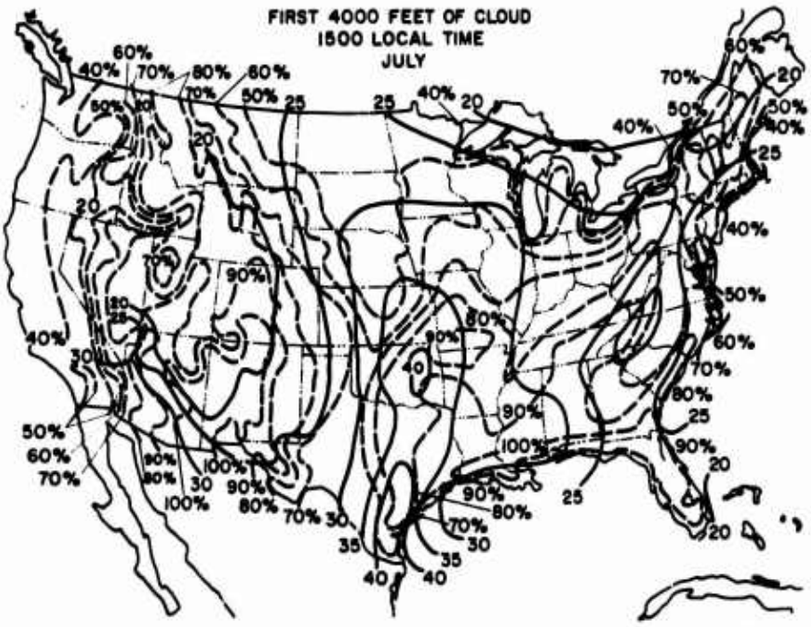

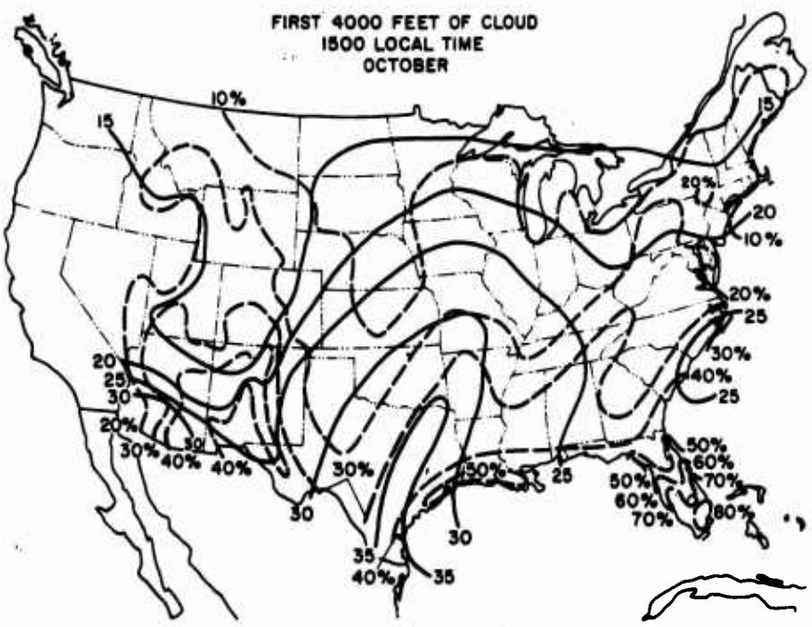

Figure 9-12 (Cont.) Percent Frequency of Cumulus and Cumulonibus Cloud (Dashed Contours) and Δ N, the Average Change in Refractive Modulus (Solid Contours) for January, April, July and October

of negative height-gradient of N in association with regions in which the temperature gradient is positive (or less negative) than the gradients of the layers just above and below are known as subsidence inversion layers. These layers generally have a large horizontal extent. Layers in close proximity to the earth's surface are strongly influenced by the local conditions of the earth's surface and for this reason are less extensive than the layers described above.

In the inversion layer, the temperature may change by a few degrees in intervals of from fifty to a few hundred feet in altitude. This temperature change accounts for only a small change of a few N-units. However, an inversion usually indicates the presence of a humid air mass under a dry one. The transition from humid to dry air causes a marked change of N in the super-refracting layer, typically of 20 to 50 N-units; changes as pronounced as 80 N-units have been measured. Super-refracting layers may be clear-weather phenomena, or can be accompanied by haze (aerosols) in the lower air mass. Invariably they signify stable weather situations, such as occur when a high pressure center stagnates in an area.

The horizontal and temporal extent of super-refractive layers varies widely. In New England it may be only a few tens of miles. In midwestern states, the layers extend farther and may last from a half hour up to a week. In the trade-wind zones of the world, the climatic regime (manifested by steady wind directions and speeds throughout most of the year) sustains super-refracting layers which extend a few thousand miles both east to west and north to south.

9.1.5 Turbulence

It has long been recognized that the effects produced by the atmosphere upon electromagnetic waves propagating through it are a measure of the nature of the atmosphere. If the atmosphere is considered as a medium with electromagnetic properties that are random functions of space and time, then atmospheric properties can be investigated by measurements of wave propagation; these observations are called remote probing. The atmospheric (or meteorological) parameters are inferred from their influence on Eqs. 9-6 and 9-7; it is assumed that scattering is due to random fluctuations in the dielectric constant of the atmosphere. When fluctuations in the refractivity are of interest they are studied via the correlation function and its Fourier transform, the spectral density. This approach is described by Tatartski (1961 and 1967), Staras and Wheelon (1959), Hufnagle and Stanley (1964), and Strohnbehn (1968).

A locally-homogeneous isotropic turbulent model of the atmosphere is assumed, that is a model of well mixed random fluctuations. This model is restrictive and requires justification for each new application. One assumes the spectral density

$\Phi_n(\kappa)$ (the three dimensional spectrum of refractivity) is given by

$$\Phi_n(\kappa) = 0.033\, C_n^2\, \kappa^{-11/3} \exp\left(-\kappa^2/\kappa_m^2\right) \quad [\mathrm{cm}^3] \tag{9-13}$$

where $\kappa_o < \kappa < \kappa_m$. The spatial wave number, κ (cm^{-1}) is $2\pi/\ell$, ℓ is the size of the turbulent eddy or blob, κ_o is $2\pi/L_o$, L_o is the outer scale of turbulence (typically the order of 10^3 to 10^4 cm, depending on layer height), κ_m is $5.92/\ell_o$ (cm^{-1}), ℓ_o is the inner scale or turbulence, and C_n is specified by Eq. 9-14. Figure 9-13 shows the typical spectrum of irregularities, $\Phi_n(\kappa)$, and the ranges of energy input, redistribution, and dissipation. Physically, the energy is put into the turbulence from the largest scale sizes (smallest value of κ) by wind shear and convective heating; the energy-producing eddies are assumed to have a spacial wave number less than κ_o. The region between κ_o and κ_m is the redistribution (inertial) range, where energy is transferred from large eddies (small κ) to smaller eddies (larger κ) until viscous effects becomes important at $\kappa_m = 5.92/\ell_o$ and the energy is dissipated. Near the ground, ℓ_o is the order of 0.1 to 1 cm.

Once the value of C_n^2 is determined, the spectral density is known. C_n^2 may be found directly from the dimensionless structure function $D_n(r)$,

$$D_n(\vec{r}) = \overline{\left[N(\vec{r}+\vec{r}_1) - N(\vec{r}_1)\right]^2} = C_n^2\, r^{2/3} \tag{9-14}$$

where $N(\vec{r})$ is the normalized fluctuating part of the index of refraction, the bar indicates the average of the squared quantity, and r ($r >> \ell_o$) is the size of the inhomogenities determined from the difference in the values of N at two points $\vec{r}$ and $\vec{r}_1$.

At optical wavelengths, C_n is determined from temperature measurements alone;

$$C_n = 10^{-6}\,(\rho/\rho_o)\, C_T \qquad \left[\mathrm{cm}^{-1/3}\right] \tag{9-15}$$

where ρ/ρ_o is the ratio of the average atmospheric density at a given altitude to the density at sea level. The structure constant, C_T, is

$$C_T = 2.4\, \epsilon^{1/3}\, (\gamma/\beta) \qquad \left[^{\circ}\mathrm{C\ cm}^{-1/3}\right] \tag{9-16}$$

where $\epsilon(\mathrm{cm}^2\,\mathrm{s}^{-3})$ is the rate of energy per unit mass dissipated by viscous friction, γ ($^{\circ}\mathrm{C\ cm}^{-1}$) is the average vertical gradient of the potential temperature, and β (s^{-1}) is the average shear rate of the wind (Haufnagle and Stanley, 1964).

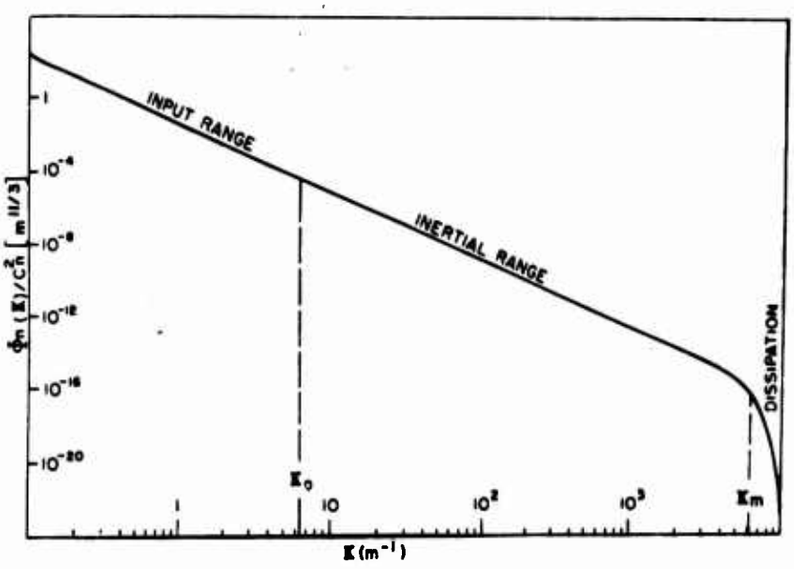

Figure 9-13. Three-dimensional Spectrum of Refractive Index Fluctuations. Note that units for the ordinate scale are $m^{11/3}$. (After Strohnbehn, 1968.)

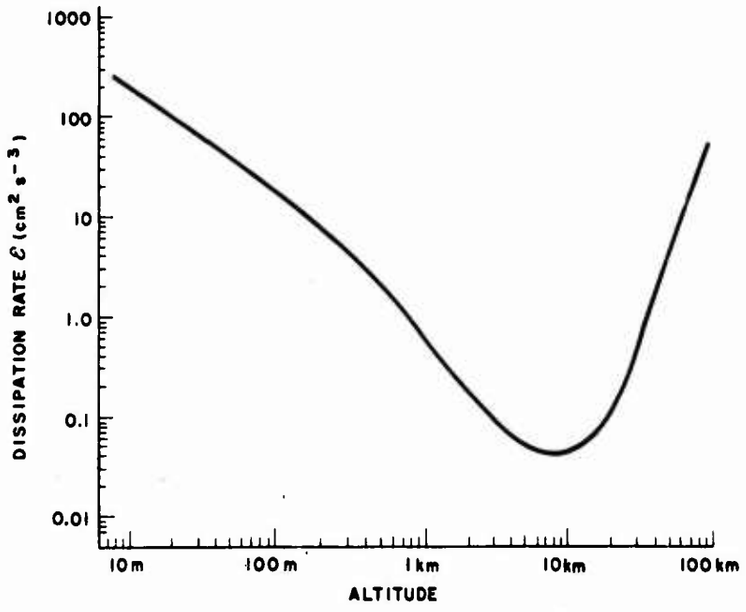

Figure 9-14. Dissipation Rate ϵ vs Altitude. The curve corresponds to an estimated average ϵ. (After Hufnagel and Stanley, 1964.)

Figure 9-14 shows the average dissipation rate estimated from observed values as a function of altitude. Figures 9-15 and 9-16 are plots of observed geometric-mean values of γ and β respectively as functions of altitude. The values of γ are taken from the 1966 Supplementary Atmosphere; the values of β are computed from reported wind profiles. Figure 9-17 shows C_n as a function of altitude; the values of ρ/ρ_o are taken from the 1966 Supplementary Atmosphere. At radio wavelengths, Eq. 9-15 cannot be used because water vapor must be considered as well as temperature (Crane, 1968).

C_n for a model atmosphere can be obtained directly from Figure 9-17. When values of ρ/ρ_o are known from radiosonde observations, C_n for the given ρ/ρ_o can be calculated by using values obtained from Figures 9-14 through 9-16 in Eqs. 9-15 and 9-16. The most accurate determination of C_n, however, is obtained from back-scatter measurements.

Tropospheric scatter experiments are used to probe the atmosphere, see Staras and Wheelon (1959) and Hardy and Katz (1969). At radio frequencies, the mechanism responsible for backscatter and forward scatter beyond the horizon is the refractive index variation due to fluctuations in properties of the atmosphere. The ratio of the received-to-transmitted power (P_r/P_t) depends upon the integral of the scattering cross section per unit volume over the common volume defined by the antenna pattern or patterns for backscatter and forward scatter respectively.

$$P_r/P_t = (\lambda^2/4\pi^2) \int_{\text{Volume}} (G_t G_r/R_1^2 R_2^2)\, \mu\, d^3r \qquad (9\text{-}17)$$

where λ is the wavelength employed, G_t and G_r are the gains of the transmitting and receiving antennas respectively, R_1 and R_2 are the distances from the scattering volume (d^3r) to the respective antennas, and μ (a reciprocal length) is the scattering cross section per unit volume. Figure 9-18 illustrates the path geometry for Eq. 9-16.

The scattering cross section per unit volume is directly related to the spectral density:

$$\mu = (\pi^2/\lambda^4)\, \Phi_n(\kappa) \qquad (9\text{-}18)$$

where $|\kappa|$ is $(4\pi/\lambda) \sin(\theta/2)$.

Scattering is not the only effect of atmospheric turbulence on the propagation of electromagnetic waves. As the waves propagate through the atmosphere, fluctuations in amplitude and phase occur. The amplitude and phase fluctuations

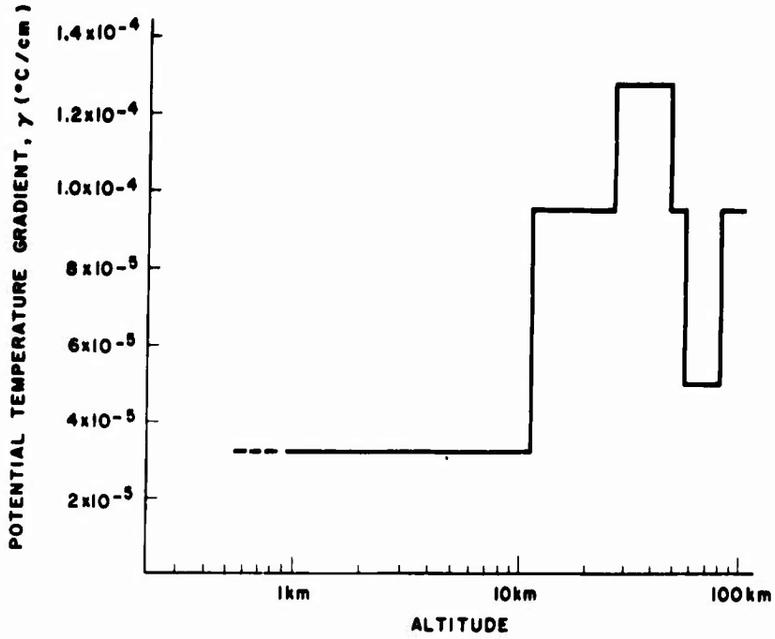

Figure 9-15. Average Potential Temperature Gradient (γ) vs Altitude. Computed from the U.S. Standard Atmosphere. (After Hufnagel and Stanley, 1964.)

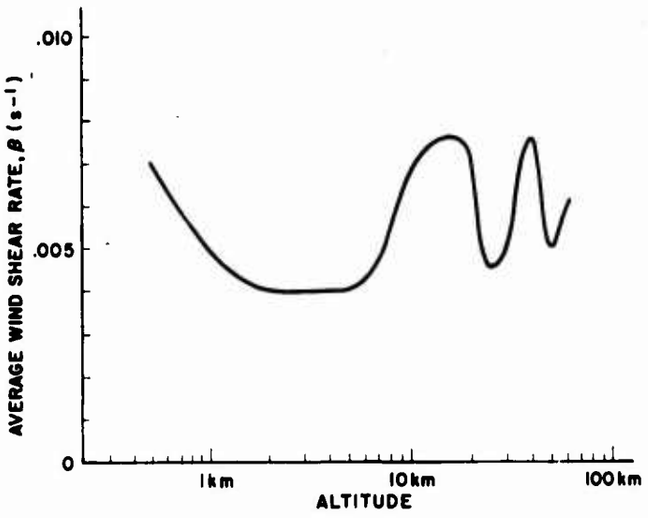

Figure 9-16. Average Wind Shear (β) vs Altitude. Computed for 0.5-km vertical separations. (From Hufnagel and Stanley, 1964.)

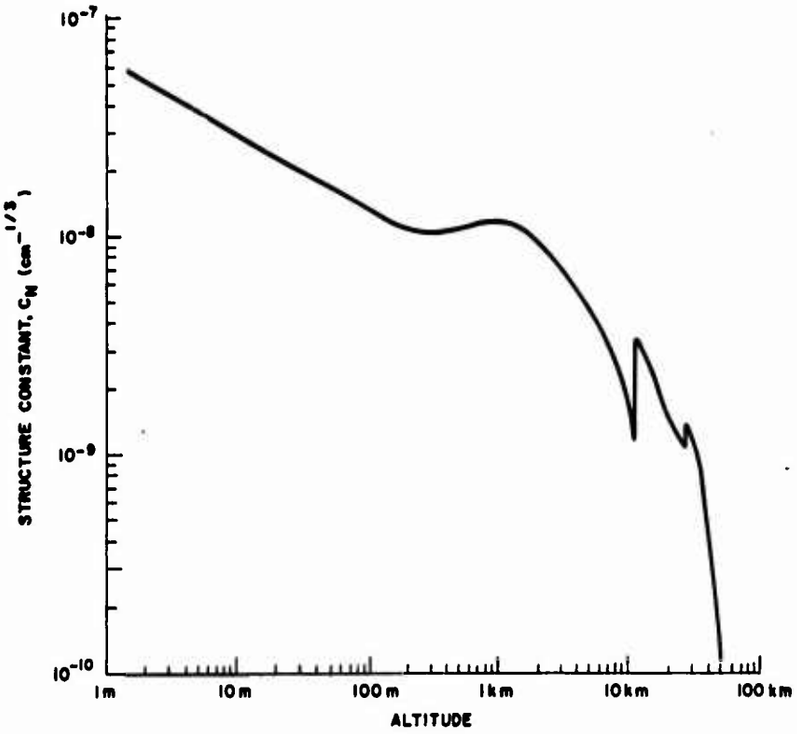

Figure 9-17. Index of Refraction Structure Constant (C_n) vs Altitude. (From Hufnagel and Stanley, 1964.)

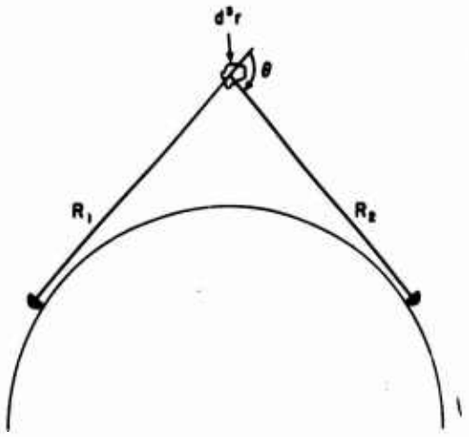

Figure 9-18. Geometry for Turbulent Scattering. R_1 and R_2 are the distances from the scattering volume d^3r to the transmitter and receiver, respectively, and Θ is the scattering angle

may be described using the equations of geometrical optics or the smooth perturbation solution of the full wave equation, see Tatarski (1961), a summary of which follows.

In order to apply the geometrical optics approximation, the conditions that have to be satisfied are:

$$\lambda << \ell_o \quad \text{and} \quad (\lambda L)^{1/2} << \ell_o ,$$

where λ is the wavelength of the propagating wave, ℓ_o is the inner scale of turbulence, and L is the path length over which the wave propagates. The phase fluctuation at a point r along the path is

$$S(\vec{r}) = k \int_0^r n(\vec{s})\, ds \tag{9-19}$$

where $S(\vec{r})$ is the total phase change, k is $2\pi/\lambda$, $n(\vec{s})$ is the index of refraction in the direction of $\vec{s}$, and ds is the element of path length. The amplitude fluctuation, χ, at point $\vec{r}$ along the path is

$$\chi = \ell n \left[A(\vec{r}) / A_o(\vec{r}) \right]$$

$$\chi = \frac{1}{2k} \int_0^x \nabla_T^2 S_1(\xi, y, z)\, d\xi \tag{9-20}$$

where $A(\vec{r})$ is total amplitude at point $\vec{r}$, ∇_T^2 is the transverse Laplacian, and ξ is the direction of propagation. $S_1(\xi, y, z)$ is the phase fluctuation about its mean value,

$$S_1(\vec{r}) = k \int_0^r \delta n(\vec{s})\, ds \tag{9-21}$$

where $\delta n(\vec{s})$ is the deviation of the index of refraction from its mean value. If $n(\vec{s})$ depends only on altitude, then Eq. 19 may be used to determine the average phase change by substituting the average index of refraction in the integrand, $k \int_0^r \langle n(\vec{s}) \rangle\, ds$; this is useful in studying refraction.

The covariance function of phase fluctuations, $C_s(\zeta)$, at two receivers that are both an equal distance L away from the transmitter and are separated from

each other by a distance $\zeta = (y^2 + z^2)^{1/2}$ is

$$C_s(\zeta) = 2\pi \int_0^\infty F_s(\kappa) J_o(\kappa\zeta) \kappa d\kappa \tag{9-22}$$

$J_o(\kappa\zeta)$ is the Bessel function and $F_s(\kappa)$ is the two dimensional Fourier transforms of $C_s(\zeta)$;

$$F_s(\kappa) = 2\pi k^2 L \Phi_n(\kappa) \qquad [cm^2] \tag{9-23}$$

The covariance function of amplitude fluctuations, $C_\chi(\zeta)$, for the conditions given above is

$$C_\chi(\zeta) = 2\pi \int_0^\infty F_\chi(\kappa) J_o(\kappa\zeta) \kappa d\kappa \tag{9-24}$$

and

$$F_\chi(\kappa) = (\pi \Lambda^3/6) \kappa^4 \Phi_n(\kappa) \qquad [cm^2] \tag{9-25}$$

Under restrictions that $\lambda << \ell_o$ and that $L << \ell_o^4/\lambda^3$, the smooth perturbation solution of the full wave equation leads to

$$F_s(\kappa) = \pi k^2 L \left(1 + \frac{\sin\alpha}{\alpha}\right) \Phi_n(\kappa) \qquad [cm^2] \tag{9-26}$$

and

$$F_\chi(\kappa) = \pi k^2 L \left(1 - \frac{\sin\alpha}{\alpha}\right) \Phi_n(\kappa) \qquad [cm^2] \tag{9-27}$$

where α is $\kappa^2 L/k$. These restrictions limit the validity of Eqs. 9-26 and 9-27 to wavelengths in the millimeter and optical regions and to relatively short paths, although in certain cases these restrictions may be relaxed, for example for $\lambda \geq \ell_o$. C and F can be measured only over a finite range of values of κ, therefore a complete knowledge of C or of F is not possible.

9.2 ATTENUATION AND BACKSCATTERING IN THE TROPOSPHERE by R. Dyer

Scattering and attenuation are in general complicated functions of particle size and dielectric properties. The square root of the dielectric constant, m, is

$$\sqrt{m} \equiv n - i\kappa \qquad (9\text{-}28)$$

where n is the phase refractive index and κ the absorption index of the medium. i is $\sqrt{-1}$.

9.2.1 Dielectric Properties

It is convenient to use the parameter K, defined by

$$K \equiv \frac{m - 1}{m + 2} , \qquad (9\text{-}29)$$

in describing the dielectric properties of the troposphere. When the wavelength is long in comparison with the size of the particles (Rayleigh approximation), the backscatter and absorption are relatively simple functions of K. In this special case, backscatter is proportional to $|K|^2$, and the attenuation is proportional to the imaginary part of minus K, Im(-K).

The variation of the dielectric characteristics of water with temperature and wavelength have been tabulated by Gunn and East (1954). For water, $|K|^2$ is practically constant; over a wide range of temperatures and wavelengths in the centimeter range $|K|^2 = 0.93$. Similarly, $|K|^2 = 0.176$ for ice of normal density (0.917 g/cm^3).

9.2.2 Backscattering and Attenuation Cross Sections

The echo power returned by a scattering particle is proportional to its backscattering cross section, σ. The power removed by an attenuating particle is proportional to the total absorption cross section, Q_t. The size parameter (electrical size) is $\pi D/\lambda$; D is the particle diameter and λ the wavelength of the incident radiation. When the diameter of the scattering or attenuating particle is small with respect to λ, the backscattering and total absorption cross sections may be expressed with sufficient accuracy by the Rayleigh approximation (molecular scattering, see Section 7.4).

For spherical particles, if $\pi D/\lambda < 0.2$,

$$\sigma = \frac{\pi^5 |K|^2 D^6}{\lambda^4} \qquad [\text{cm}^2] . \qquad (9\text{-}30)$$

For particles with $\pi D/\lambda > 0.2$, σ should be computed from the equations of the Mie theory of scattering (Battan, 1959). Figures 9-19 and 9-20 show normalized backscattering cross section ($4\sigma/\pi D^2$) for ice and for water versus the size parameter,

computed from the exact Mie equations. The normalized curve for ice is invariant with wavelength in the microwave region; the normalized curve for water is for water at 0°C at 3.2-cm wavelength. As Figures 9-19 and 9-20 show, ice spheres equal to or larger than the wavelength may scatter more than an order of magnitude greater than water spheres of the same size; this is confirmed by experimental measurements (Atlas et al., 1960).

Measurements at 5 cm wavelength indicate that the backscattering of so-called "spongy" hail (a mixture of ice and water) is 3 to 4 dB above that of the equivalent all-water spheres and at least 10 dB above that of the equivalent solid ice spheres (Atlas et al., 1964). Because of the variabilities of sizes, shapes, and liquid water content of hail, no general rules concerning backscattering and attenuation cross sections for hail can be made. As a first approximation, however, the ice curve of Figures 9-19 and 9-20 may be used.

For spherical particles, if $\pi D/\lambda < 0.1$,

$$Q_t = \frac{\pi^2 D^3}{\lambda} \text{ Im } (-K) + \frac{2}{3}\sigma \quad [\text{cm}^2] \,. \tag{9-31}$$

When $\pi D/\lambda > 0.1$, Q_t must also be computed from the exact Mie equations. Figure 9-21 presents curves of the normalized total attenuation cross section ($4Q_t/\pi D^2$) for water at 0°C at two wavelengths. Figure 9-22 shows the normalized total attenuation cross section for ice.

9.2.3 Reflectivity

The average echo power returned by a group of randomly distributed scattering particles is proportional to their reflectivity, η. Reflectivity is defined as the summation of the backscatter cross sections of the particles over a unit volume; $\eta \equiv \Sigma\sigma$. When the backscattering particles are spheres and are small enough with respect to wavelength so that the Rayleigh approximation can be used (that is $\pi D/\lambda < 0.2$), the reflectivity is proportional to the radar reflectivity factor, Z, which is the summation over a unit volume of the sixth power of the particle diameters; $Z \equiv \Sigma D^6$. Summation over a unit volume of Eq. (9-30) gives,

$$\Sigma\sigma = \eta = \frac{\pi^5 |K|^2 Z}{\lambda^4} \times 10^{-12} \quad [\text{cm}^{-1}) \tag{9-32}$$

for Z in conventional units of $\text{mm}^6\ \text{m}^{-3}$ and λ in centimeters.

When the particles are larger than Rayleigh size or composed of ice or water-ice mixtures, it is common practice to measure the radar reflectivity and express

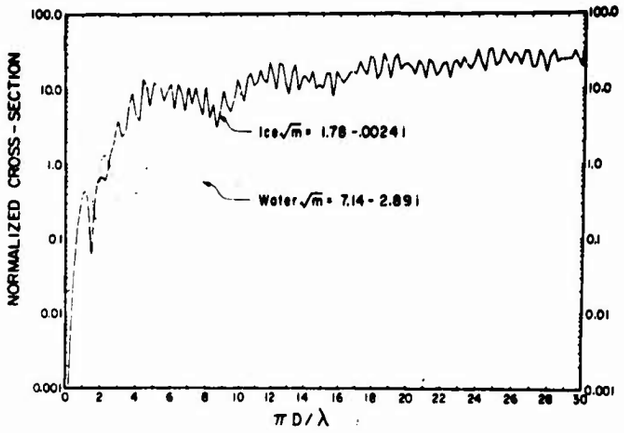

Figure 9-19. Calculated Values of the Normalized ($4\sigma/\pi D^2$) Backscatter Cross Section for Water at 3.21 cm and 0°C and for Ice at Wavelengths from 1 to 10 cm

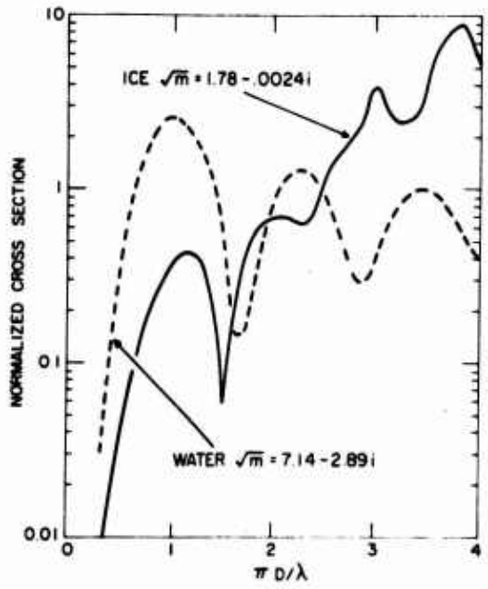

Figure 9-20. Calculated Values of the Normalized ($4\sigma/\pi D^2$) Backscatter Cross Section for Water at 3.21 cm and 0°C and for Ice at Wavelengths from 1 to 10 cm (Detail of Figure 9-19.)

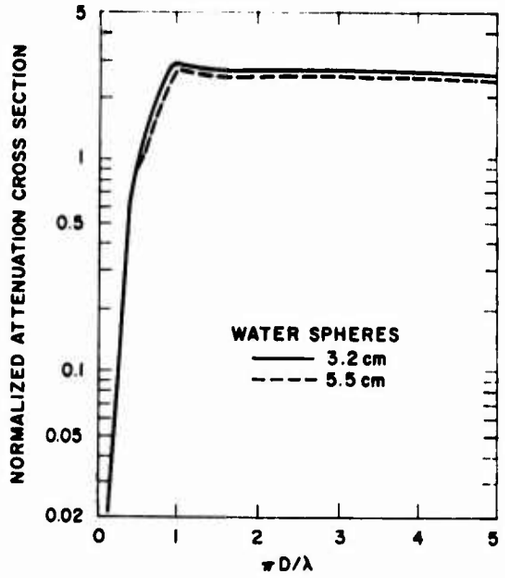

Figure 9-21. Normalized $(4Q_t/\pi D^2$ Attenuation Cross Sections of Water Spheres at 0°C and Wavelengths of 3.2 and 5.5 cm. (After B.M. Herman, S.R. Browning and L.J. Battan, Tech. Rept. No. 9, Institute of Atmospheric Physics, University of Arizona, 1961.)

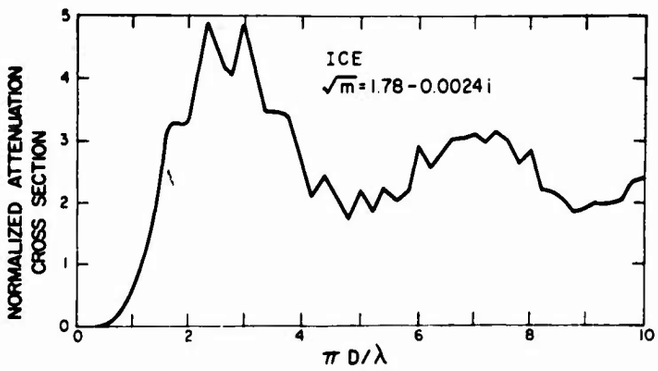

Figure 9-22. Normalized $(4Q_t/\pi D^2$ Attenuation Cross Sections of Ice Spheres at Wavelengths Between 1 and 10 cm. (After B.M. Herman and L.J. Battan, Proc. Ninth Weather Radar Conference, Amer. Meteorological Society, p. 259, 1961.)

it in terms of an equivalent reflectivity factor, Z_e. By substituting $|K|^2 = 0.93$ (water in the centimeter wavelength range) in Eq. (9-32).

$$Z_e = 3.5 \times 10^9 \lambda^4 \eta \qquad [mm^6 m^{-3}] . \tag{9-33}$$

Thus Z_e is simply ΣD^6 of water drops of Rayleigh size that would have the same reflectivity as that measured.

Because Z is a meteorological parameter that depends only on the particle size distribution and concentration, it is useful to express Z as a function of the precipitation rate, R. Table 5-5 (Section 5.2 Chapter 5 Revised, Air Force Surveys in Geophysics No. 212 , AFCRL-69-0487 , October 1969) lists Z as a function of R for various types of rain at various locations in the Northern Hemisphere.

The scattering properties of snow are complex. Snow may occur in a great variety of forms of either single ice crystals or aggregates of such crystals. Measurements suggest the following relationships are reasonable:

$$Z = 500 R^{1.6}, \text{ for single crystals} \tag{9-34}$$

and

$$Z = 2000 R^{2.0}, \text{ for aggregates} \tag{9-35}$$

R is the snowfall rate in millimeters of water per hour.

Carlson (1968) suggests that a reasonable average for all types of snow measured aloft would be

$$Z = 1000 R^{2.67} \tag{9-36}$$

Clouds composed of water particles scatter very poorly. Nevertheless, high-power, short-wavelength radars may sometimes detect water clouds at short ranges. An empirical relationship for water clouds is

$$Z = 0.048 M^2, \tag{9-37}$$

where M, the water content, is in grams per cubic meter.

The reflectivity of ice clouds is not known. However, many so-called ice clouds are really snow crystals falling and evaporating in a dry layer below the cloud base.

9.2.4 Attenuation

I_r, the intensity of radiation after travelling a distance r through an atmospheric path of constant attenuation, can be related to the initial intensity I_o by a power law,

$$I_r = I_o \, 10^{-Ar/10} ; \qquad (9\text{-}38)$$

A is the attenuation coefficient in units of dB per kilometer, and r is in kilometers. A is the sum of the attenuation coefficient due to precipitation (A_p), the attenuation coefficient due to clouds (A_c), and the attenuation coefficient due to atmospheric gases (A_a); $A = A_p + A_c + A_a$. For radar (two-way transmission), the distance r is twice the range (twice the path length from source to target).

9.2.4.1 ATTENUATION BY PRECIPITATION

In recent years, measurements of the rainfall attenuation in the millimeter and centimeter wavelength range have been consistently higher than the attenuations predicted theoretically. Much of the discrepancy, however, is probably caused by an inadequate representation of the rain field during the attenuation experiments. Figure 9-23 shows a summary of the results of 12 such investigations at 10 different wavelengths between 4.3 mm and 3.2 cm. The solid lines show the maximum and minimum measured attenuation coefficients per unit rainfall rate. The dashed line is the measured mean, and the hatched line is the mean that would have been predicted from theory. Attenuation is a function of temperature as well as of wavelength and precipitation rate (or, more exactly, drop size distribution). However, the variability in the measured attenuations exceeds the temperature correction, and it is reasonable to assume (Medhurst, 1965) that the attenuation coefficient is a linear function of rainfall rate. Measurements of the attenuation caused by snow are difficult to obtain because the effect is so small. Figure 9-24 shows the theoretical maximum attenuation coefficients assuming a maximum snowfall rate of 10 mm of water per hour. Because snowfall rates seldom exceed 3 mmw h^{-1}, attenuation due to snow should generally be one-third or less the value shown in Figure 9-24. For more exact computations of the attenuation to be expected at various temperatures, wavelengths and snowfall rates, see Gunn and East (1954).

9.2.4.2 ATTENUATION BY CLOUDS

Attenuation by clouds depends on the liquid water content, the temperature, and whether the cloud is composed of ice or water particles. Figure 9-25 gives representative attenuations per unit water content of clouds composed entirely of water particles, and of clouds composed of ice crystals. Note the temperature

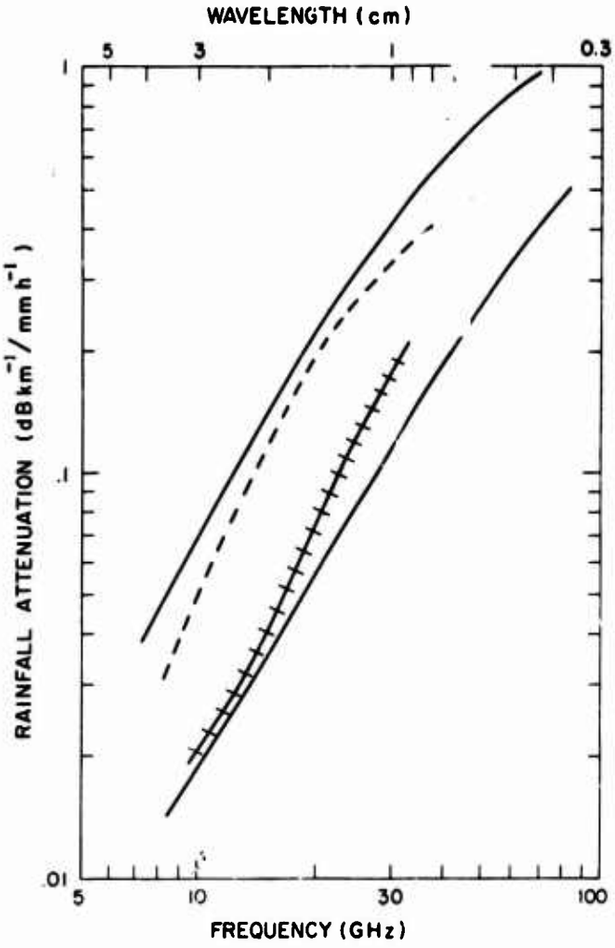

Figure 9-23. Attenuation (dB/km) per Unit Rainfall Rate (mm/h) as a Function of Wavelength. The solid lines are the maximum and minimum attenuations measured at each wavelength, the dashed line is the mean of the measurements, and the hatched line is the mean predicted from theory. (After Medhurst, 1965)

and wavelength dependence, and the sharp decrease in attenuation in going from the liquid to the solid phase.

9.2.4.3 ATTENUATION BY ATMOSPHERIC GASES

Molecular oxygen and water vapor are the only atmospheric gases causing measurable attenuation of microwaves. Atmospheric pressure, temperature, and water-vapor content are the governing variables. There is an oxygen absorption

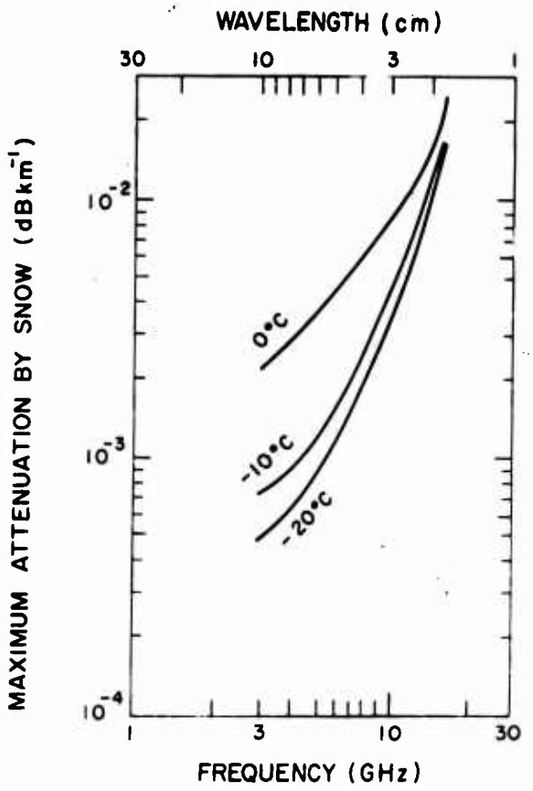

Figure 9-24. Theoretical Attenuation Due to Snowfall of 10 mm of Water Content per Hour as a Function of Wavelength and Temperature. Snowfall rates rarely exceed 3 mm of water content per hour, hence usual attenuations should be approximately one-third or less of these maximum values

line at 0.5 cm and a water vapor absorption line at 1.35 cm. Table 9-1 shows the variation of attenuation by oxygen with wavelength (0.7 to 10 cm) at 20°C and one-atmosphere pressure. Attenuation by oxygen is pressure and temperature dependent; it increases slowly as the temperature decreases, and increases as the square of the pressure. Table 9-2 lists correction factors to be used at various temperatures. The attenuation given in Table 9-1 must be multiplied by a factor given in Table 9-2 in order to correct for pressure and temperature whenever these variables are not equal to 20°C and one-atmosphere respectively. Both Tables 9-1 and 9-2 assume a constant ratio of molecular oxygen to other atmospheric gases; this assumption is valid up to altitudes of approximately 80 km.

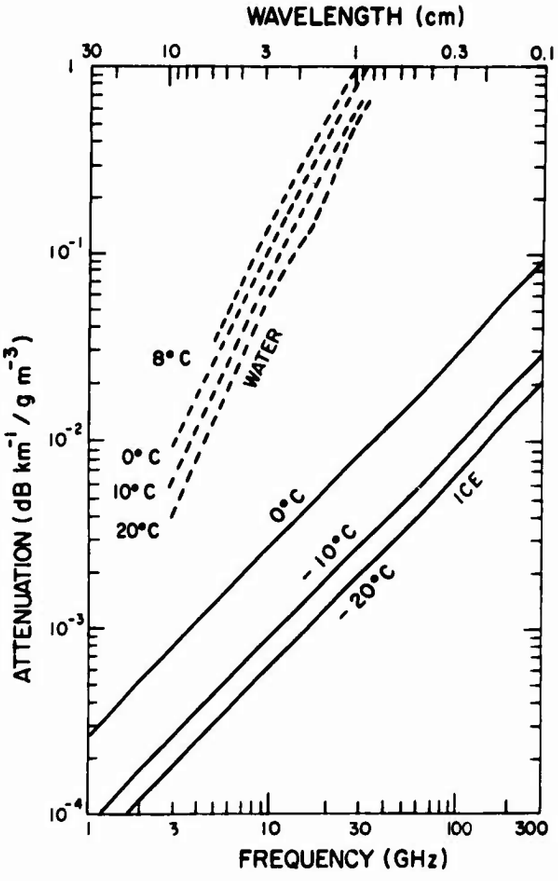

Figure 9-25. Attenuation (dB/km) per Unit Water-content (g/m^3) of Ice and Water Clouds as a Function of Wavelength and Temperature. The solid lines are the attenuation curves for clouds composed of ice particles, and the dashed curves are for water clouds

Water vapor is a much more variable constituent of the atmosphere than oxygen. Table 9-3 tabulates the attenuation as a function of temperature and wavelength (Gunn and East, 1954); the relation is only approximate for operating wavelengths in the vicinity of 1.35 cm because of the water vapor absorption line at 1.35 cm.

Table 9-1. Attenuation Due to Molecular Oxygen at a Temperature of 20°C and a Pressure of 1-Atmosphere

Wavelength (cm)	Attenuation (dB / km)
10	6.5×10^{-3}
7.5	7.0×10^{-3}
3.2	7.2×10^{-3}
1.8	7.5×10^{-3}
1.5	8.5×10^{-3}
1.25	1.4×10^{-2}
0.8	7.5×10^{-2}
0.7	1.9×10^{0}

Table 9-2. Correction Factors for Oxygen Attenuation

Temperature (°C)	Correction Factor*
20	$1.00\ P^2$
0	$1.19\ P^2$
-20	$1.45\ P^2$
-40	$1.78\ P^2$

*P is pressure in atmospheres.

Table 9-3. Water-vapor Attenuation in dB per Kilometer*

Wavelength (cm)	Temperature			
	20°C	0°C	-20°C	-40°C
10	$7 \quad PW \times 10^{-5}$	$8 \quad PW \times 10^{-5}$	$9 \quad PW \times 10^{-5}$	$10 \quad PW \times 10^{-5}$
5.7	$2.4 \quad PW \times 10^{-4}$	$2.7 \quad PW \times 10^{-4}$	$3.0 \quad PW \times 10^{-4}$	$3.4 \quad PW \times 10^{-4}$
3.2	$7 \quad PW \times 10^{-4}$	$8 \quad PW \times 10^{-4}$	$9 \quad PW \times 10^{-4}$	$10 \quad PW \times 10^{-4}$
1.8	$4.3 \quad PW \times 10^{-3}$	$4.8 \quad PW \times 10^{-3}$	$5.0 \quad PW \times 10^{-3}$	$5.4 \quad PW \times 10^{-3}$
1.24	$2.2 \quad PW \times 10^{-2}$	$2.33 \quad PW \times 10^{-2}$	$2.46 \quad PW \times 10^{-2}$	$2.61 \quad PW \times 10^{-2}$
0.9	$9.5 \quad PW \times 10^{-3}$	$1.04 \quad PW \times 10^{-2}$	$1.14 \quad PW \times 10^{-2}$	$1.26 \quad PW \times 10^{-2}$

* P is pressure in atmospheres and
W is water-vapor content in grams per cubic meter.

References

Atlas, D., Harper, W.G., Ludlam, F.H., and Macklin, W.C. (1960) Radar Scatter by Large Hail, Quart. J. Roy. Meteorol. Soc. 86:468.

Atlas, D., Hardy, K.R., and Joss, J. (1964) Radar Reflectivity of Storms Containing Spongy Hail, J. Geophys. Res., 69:1955.

Battan, L.J. (1959) Radar Meteorology, The University of Chicago Press, p. 33.

Bean, B.R., and Dutton, E.J. (1968) Radio Meteorology, Dover Publishing Co.

Carlson, P.E. (1968) Measurement of Snowfall by Radar, McGill University Stormy Weather Group Scientific Report MW-54.

Crane, R.K. (1968) Monostatic and Bistatic Scattering from Thin Turbulent Layers in the Atmosphere, Lincoln Laboratory Tech. Note 1968-34, (ESD-TR-68-267).

Cunningham, R.M. (1962) Cumulus Climatology and Refractive Index Studies II, Geophys. Res. Papers No. 51, AFCRL.

Edlen, B. (1953) Dispersion of Standard Air, J. Opt. Soc. Am., 43:339

Gunn, K.L.S., and East, T.W.R. (1954) The Microwave Properties of Precipitation Particles, Quart. J. Roy. Meteorol. Soc. 80:522.

Hardy, K.R., and Katz, I. (1969) Probing the Clear Atmosphere with High Power High Resolution Radars, PROC. IEEE 57:468.

Hufnagle, R.E., and Stanley, N.R. (1964) Modulation Transfer Function Associated with Image Transmission Through Turbulent Media, J. Opt. Soc. Am. 54:52.

Medhurst, R.G. (1965) Rainfall Attenuation of Centimeter Waves: Comparison of Theory and Measurement, IEEE Trans. on Antennas and Propagation AP-13:550.

Staras, H., and Wheelon, A.D. (1959) Theoretical Research on Tropospheric Scatter Propagation in the United States 1954-1957, IEEE Trans. Antennas and Propagation AP-7:80.

Strohnbehn, J.W. (1968) Line of Sight Wave Propagation Through the Turbulent Atmosphere PROC. IEEE 56:1301.

Tatarski, V.I. (1961) Wave Propagation in a Turbulent Media, Chapters 3, 6 and 7, McGraw-Hill, New York.

Tatarski, V.I. (1967) Propagation of Waves in a Turbulent Atmosphere (in Russian) Moscow, Nanka.

Unclassified
Security Classification

DOCUMENT CONTROL DATA - R&D

(Security classification of title, body of abstract and indexing annotation must be entered when the overall report is classified)

1. ORIGINATING ACTIVITY *(Corporate author)* Air Force Cambridge Research Laboratories (ECS) L. G. Hanscom Field Bedford, Massachusetts 01730	2a. REPORT SECURITY CLASSIFICATION Unclassified 2b. GROUP

3. REPORT TITLE
REFRACTION, ATTENUATION, AND BACKSCATTERING OF ELECTROMAGNETIC WAVES IN THE TROPOSPHERE: A Revision of Chapter 9, Handbook of Geophysics and Space Environments

4. DESCRIPTIVE NOTES *(Type of report and inclusive dates)*
Scientific. Interim.

5. AUTHOR(S) *(First name, middle initial, last name)*
V. J. Falcone, Jr.
R. Dyer

6. REPORT DATE January 1970	7a. TOTAL NO. OF PAGES 38	7b. NO. OF REFS 16
8a. CONTRACT OR GRANT NO. b. PROJECT, TASK, WORK UNIT NOS. None c. DOD ELEMENT d. DOD SUBELEMENT	9a. ORIGINATOR'S REPORT NUMBER(S) AFCRL-70-0007 9b. OTHER REPORT NO(S) *(Any other numbers that may be assigned this report)* AFSG No. 214	

10. DISTRIBUTION STATEMENT
1—This document has been approved for public release and sale; its distribution is unlimited.

11. SUPPLEMENTARY NOTES TECH, OTHER	12. SPONSORING MILITARY ACTIVITY Air Force Cambridge Research Laboratories (ECS) L. G. Hanscom Field Bedford, Massachusetts 01730

13. ABSTRACT

The need for geophysical and astrophysical information is critical for the design of aircraft, missiles, and satellites. The HANDBOOK OF GEOPHYSICS AND SPACE ENVIRONMENTS is an attempt by the U. S. Air Force to organize some of these data into compact form.

The effects of the lower atmosphere on propagation of electromagnetic waves in the optical, microwave, and radio regions are discussed in this Chapter; the emphasis is on information useful in meteorological investigations.

DD FORM 1 NOV 68 1473

Unclassified
Security Classification

14. KEY WORDS	LINK A		LINK B		LINK C	
	ROLE	WT	ROLE	WT	ROLE	WT
atmosphere, attenuation coefficients atmosphere, scattering cross sections backscattering, tropospheric electromagnetic propagation, atmospheric effects refractive modulus, atmosphere						